Biomaterials Science

ROYAL SOCIETY OF CHEMISTRY

PAPER

View Article Online
View Journal | View Issue

Cite this: *Biomater. Sci.*, 2020, **8**, 4616

Broad spectrum antibacterial photodynamic and photothermal therapy achieved with indocyanine green loaded SPIONs under near infrared irradiation†

K. Bilici,‡[a] N. Atac,‡[b] A. Muti,‡[c] I. Baylam,[d] O. Dogan,[b] A. Sennaroglu,*[c,d] F. Can*[b] and H. Yagci Acar *[a,d]

Antimicrobial photodynamic therapy (aPDT) and antimicrobial photothermal therapy (aPTT) are promising local and effective alternative therapies for antibiotic resistant bacterial infections and biofilms. A combination of nanoparticles and organic photosensitizers offers a great opportunity to combine PDT and PTT for effective eradication of both planktonic bacteria and their biofilms. In this work, photo-induced antibacterial activity of indocyanine green (ICG), 3-aminopropylsilane coated superparamagnetic iron oxide nanoparticles (APTMS@SPIONs) and ICG loaded APTMS@SPIONs was evaluated on planktonic cells and biofilms of Gram-negative (*E. coli*, *K. pneumoniae*, *P. aeruginosa*) and Gram-positive (*S. epidermis*) bacteria. A relatively low dose of ICG (25 μg mL^{-1}) and SPIONs (0.425 μg mL^{-1} nanoparticle) in combination with single, short (10 min) laser irradiation at 808 nm with a power of 1150 mW was used in this study. No dark toxicity of the agents or antibacterial effect of the laser irradiation was observed. The charge of the particles did not provide a significant difference in their penetration to Gram-negative *versus* Gram-positive bacterial strains or their biofilms. APTMS@SPION/laser treatment completely eliminated *P. aeruginosa* and provided 7-log reduction in the colony forming unit (CFU) of *E. Coli*, but was not effective on the other two bacteria. This is the first example for antibacterial phototoxicity of this nanoparticle. ICG/laser and ICG-APTMS@SPION/laser treatments provided complete killing of all planktonic cells. Successful eradication of all biofilms was achieved with ICG/laser (3.2–3.7 log reduction in CFUs) or ICG-APTMS@SPION/laser treatment (3.3–4.4 log reduction in CFUs). However, an exceptionally high, 6.5-log reduction as well as a dramatic difference between ICG *versus* ICG/APTMS@SPION treatment was observed in *K. pneumoniae* biofilms with ICG-APTMS@SPION/laser treatment. Investigation of the ROS production and increase in the local temperature of the biofilms that were subjected to phototherapy suggested a combination of aPTT and aPDT mechanisms for phototoxicity, exhibiting a synergistic effect when ICG-APTMS@SPION/laser was used. This approach opens an exciting and novel avenue in the fight against drug resistant infections by successfully utilizing the antimicrobial and antibiofilm activity of low dose FDA approved optically traceable ICG and relatively low cost clinically acceptable iron oxide nanoparticles to enable effective aPDT/aPTT combination, induced *via* short-duration laser irradiation at a near-infrared wavelength.

Received 18th May 2020,
Accepted 4th July 2020

DOI: 10.1039/d0bm00821d

rsc.li/biomaterials-science

Antibiotic resistance has become a significant threat due to the emergence of multidrug resistant pathogens and limited therapy options.[1] Multidrug resistant pathogens are subject of concern because of high fatality rates due to infections in health care settings. The multidrug resistance rates were reported as 59% in *E. coli*,[2] 50% in *K. pneumoniae*,[3] 31.4% in *S. epidermidis*[4] and 20.6% in *P. aeruginosa.*[5] Biofilm production of these bacteria also increases the risk of treatment failure. Antibiotics cannot efficiently penetrate through the biofilm matrix[6] and thus result in persistence of bacteria, promote positive selection, and spread of antimicrobial resistance.[7]

[a]*Koc University, Department of Chemistry, Rumelifeneri Yolu, Sariyer 34450, Istanbul, Turkey. E-mail: fyagci@ku.edu.tr, fucan@ku.edu.tr; Fax: +902123381559; Tel: +902123381742*
[b]*Koç University School of Medicine, Department of Infectious Diseases and Clinical Microbiology, Topkapı, Istanbul, Turkey*
[c]*Koc University, Departments of Physics and Electrical-Electronics Engineering, Rumelifeneri Yolu, Sariyer 34450, Istanbul, Turkey*
[d]*Koc University, KUYTAM, Rumelifeneri Yolu, Sariyer 34450, Istanbul, Turkey*
†Electronic supplementary information (ESI) available. See DOI: 10.1039/d0bm00821d
‡These authors are equally contributing first authors.

Rapidly increasing antibiotic resistance and high mortality rates lead to an urgent need for new alternatives in infection therapy. Light based local therapies such as photodynamic therapy (PDT) and photothermal therapy (PTT) emerged as alternative and complementary therapeutic methods in cancer.[8–10] Anti-microbial photodynamic therapy (aPDT) has been reported since early 1990s as an alternative therapeutic approach or as a complementary method to antimicrobial drugs.[11–13] It was reported that aPDT does not cause any resistance to drugs or to aPDT and is not influenced by the drug resistance status of the microbial cells.[12] aPDT is a promising approach for the inactivation of biofilms, as well.[14] In aPDT, irradiation of a photosensitizer, which is usually a small molecule, generates reactive oxygen species (ROS), which then attack proteins, lipids, nucleic acids, *etc.*, in the vicinity to kill the bacterial cell and may damage the biofilm matrix.[15]

In recent years, photothermal therapy (PTT) has attracted a great deal of attention, following the development of photosensitive inorganic nanoparticles that cause local heating upon irradiation, especially at near infrared wavelengths (NIR) which provides deeper penetration of light. Local temperature increase causes thermal ablation of the occupied malignant tissue. Antimicrobial PTT (aPTT) has been recently shown as a promising approach for the elimination of planktonic cells and biofilms.[16–19] Disruption of the biofilm integrity *via* aPTT enhances penetration of antibacterial drugs into the biofilms, in addition to the thermal ablation of the bacteria.[20,21]

Indocyanine green (ICG), a FDA approved NIR organic dye, is used for intraoperative optical imaging in clinics[22,23] and for dental imaging.[24] It is under investigation for image-guided PDT and has been, most recently, used as a photosensitizer for combined PDT–PTT upon irradiation at 808 nm.[25–27] Long wavelength absorption of ICG and safety in the absence of light irradiation are quite attractive. However, there are some major challenges in ICG based phototherapy, including rapid clearance from the body, instability in aqueous solutions, and photobleaching.[28,29] Numerous studies have been performed to combine nanoparticles and ICG into one system that can overcome these issues.[30–32] Besides, attempts to utilize PDT–PTT combination on bacterial infections[33–35] and for cancer therapy[25,26,36] have recently emerged and shown great promise.

Superparamagnetic iron oxide nanoparticles (SPIONs) are well known for magnetic resonance imaging,[27] magnetic hyperthermia, and drug delivery.[37,38] Recently, they have also been recognized as effective PTT agents under NIR laser irradiation.[39,40] This is quite exciting since SPIONs are considered biocompatible and there are several SPION compositions that are FDA approved. Recently, we have shown the combined PTT-PDT potential of the ICG loaded 3-aminopropyltrimethoysilane (APTMS) coated SPIONs on MCF7 and HT29 cancer cell lines by employing a single laser treatment at 795 nm which demonstrated a 2-fold increase in ROS generation, resulting in nearly complete cell death.[41] SPIONs have been used to deliver bactericidal agents previously or to cause a dark bactericidal effect which required quite high doses and/or toxic coating materials which may pose serious risks in clinic transition.[42–44] But, the combined PTT-PDT approach coupled with the material choice (SPIONs and ICG presented in our previous study) is very promising for bacterial infections as well, especially for biofilms which are difficult to penetrate through.

In this study, we investigated the bactericidal effect of ICG, APTMS@SPIONs, and ICG loaded APTMS@SPIONs on planktonic cells and biofilms of Gram-negative *E. coli*, *K. pneumoniae*, *P. aeruginosa* as well as Gram-positive *S. epidermidis*, with and without NIR laser irradiation. NIR laser irradiation at 808 nm was applied at a clinically safe laser power (1150 mW) and over a practically short duration (10 minutes). Our study focused on the influence of the charge of the photosensitizers on their internalization by Gram-negative and Gram-positive bacteria and their biofilms, as well as ROS generation, and hyperthermia generated by the short irradiation of treated biofilms to evaluate the sensitivity of different bacterial strains. Our experiments indicate that a combination of ICG and SPIONs has the potential to provide an enhanced treatment of antibiotic resistant bacteria and their biofilms *via* a dual aPDT/aPTT mechanism.

Experimental methods

Materials

Iron(II) chloride, iron(III) chloride, suprapur nitric acid (65%) and suprapur sulphuric acid (96%) were purchased from Merck (purity levels 99%, Darmstadt, Germany). 3-Aminopropyltrimethoxysilane (APTMS) was purchased from Alfa Aesar (MA, USA). Cardiogreen (indocyanine green) was obtained from Sigma-Aldrich (MO, USA). Vivaspin 20 centrifugal filters (5 kDa MW cut-off) were obtained from Sartorius (Goettingen, Germany). In all experiments, only ultra-pure water was used (18.2 MΩ, Rephile Bioscience and Technology, Shanghai, China).

Preparation of ICG loaded APTMS@SPIONs

ICG loaded APTMS coated SPIONs were prepared as described in our previous work. Briefly, cationic APTMS@SPIONs were synthesized by a co-precipitation method from iron salts at Fe^{3+}/Fe^{2+} of 2/1 (mol ratio) using NH_4OH in the presence of APTMS at 85 °C under Ar flow. Produced APTMS@SPIONs were washed with DI water several times using centrifugal filters (5 kDa MW cut-off) and stored at room temperature.

To prepare ICG-APTMS@SPIONs, ICG was added dropwise to nanoparticle solution (5 mg mL^{-1}, 10 mL) at a concentration of 0.5 mg mL^{-1} and then mixed at 750 rpm for 2 h at room temperature. Then, it was washed from centrifugal filters (10 kDa MWCO). The loaded ICG amount was calculated based on the unbound ICG that was removed by the washing process using the absorbance of ICG at 780 nm and a calibration curve created with free ICG. ICG encapsulation

efficiency (EE) and loading efficiency (LE) were calculated as follows:

$$\mathrm{EE}(\%) = [\text{Weight of loaded ICG}/\text{Weight of ICG input}] \times 100$$

$$\mathrm{LE}(\%) = [\text{Weight of loaded ICG}/\text{Weight of ICG loaded SPIONs}] \times 100$$

Characterization methods

Absorbance measurements were performed with a Shimadzu UV-VIS-NIR spectrophotometer. A Malvern Zetasizer NanoZS was used to determine the hydrodynamic size and surface charge of nanoparticles. An inductively coupled plasma-mass spectrometer (Agilent 7700X ICP-MS) was used to determine the iron content of nanoparticles. Samples were etched with nitric acid (65%) and sulphuric acid (96%) for the ICP-MS measurements. Nanoparticle internalization by planktonic cells and biofilms was determined by ICP-MS after cells/biofilms were washed with fresh phosphate buffered saline (PBS) and treated with acid as explained below.

Antimicrobial activity and antibiofilm assays

Bacterial isolates. *Escherichia coli* ATCC® 25922™, *Klebsiella pneumoniae* ATCC® 700831™, *Pseudomonas aeruginosa* ATCC® 700829™ and *Staphylococcus epidermidis* ATCC® 35984™ were used in the experiments.

Antibacterial activity on planktonic bacteria. A single colony of bacteria from overnight cultures was inoculated in Tryptic Soy Broth (TSB, BD™ Bacto™) and incubated overnight at 37 °C–135 rpm. ICG, APTMS@SPIONs and ICG-APTMS@SPIONs were added to the cell suspension in a final concentration of 25 μg ml^{-1} ICG and 425 μg Fe per mL. TSB was added for control culture. Cultures were incubated at 37 °C overnight. Survival of bacteria was determined by colony counting after serial ten-fold dilutions. At least 2-log (99%) growth reduction in mean CFU ml^{-1} values was considered as significant inhibition. All studies were performed in triplicate.

Anti-biofilm activity. Biofilms were produced in 96-well plates with a protocol described by Merritt *et al.*[45] Then, media were gently removed from wells and fresh TSB-glucose or ICG, APTMS@SPIONs and ICG-APTMS@SPIONs were added into wells at 25 μg ml^{-1} ICG and 425 μg Fe per mL dose. Following overnight incubation at 37 °C, survival of bacteria was determined by colony counting as described above. At least 2-log growth reduction in mean CFU ml^{-1} values was considered as significant inhibition. All studies were performed with three replicates.

Laser irradiation protocol

During laser irradiation experiments, 96-well plates were irradiated from the bottom of the plates by using a fiber-coupled 808 nm diode laser which was operated up to an output power of 1150 mW. The laser beam emerging from the fiber bundle (diameter = 1550 μm) was imaged with the help of two convex lenses (L1 and L2 in Fig. 1 with focal lengths of $f1$ = 4 mm and $f2$ = 50 mm) with an adjustable separation, so that the spot size can be matched with the diameter of each well (7 mm). The irradiation fluence of the laser could be varied up to 3 W cm^{-2}. The fluence was determined from $J = P_L/{w_L}^2$, where P_L is the laser incident power (1150 mW) on each well and w_L is the radius of the laser beam which was matched to the radius of the well (3.5 mm). The samples were kept inside a plexiglass box whose temperature was maintained at 37 °C with a closed-loop heater. During laser irradiation experiments, the temperature rise of each well was monitored with a thermal camera which was positioned above the plexiglass box. Since plexiglass is not transparent at infrared (IR) wavelengths (8–10 μm) radiated from an object at temperatures of 37 °C and above, a circular hole with a diameter of 64 mm was punched on the top panel of the plexiglass box to capture the IR signal with the camera. For the same reason, the polystyrene well-plate cover was replaced with a GaAs wafer which is transparent in this wavelength range. The IR transmission of the GaAs wafer was further taken into account to perform calibrated temperature measurements.

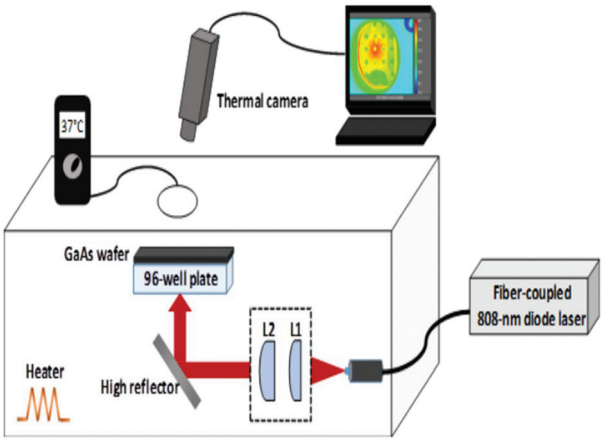

Fig. 1 A schematic of the experimental setup which was used during the laser irradiation of bacteria.

Laser treatment of bacteria

Both planktonic bacteria and biofilms grown in well-plates were irradiated with a near infrared laser (808 nm) with 1150 mW output power for 10 minutes from the bottom of the plates. Following the laser treatment, planktonic cells and biofilms were incubated at 37 °C for 24 hours and survival of both planktonic and biofilm cells was evaluated by using the same protocol as described above.

Intracellular ROS detection

Bacterial biofilms were produced as described above, treated with APTMS@SPIONs, ICG, and ICG-APTMS@SPIONs for 24 hours, separately, and exposed to an 808 nm laser with a power of 1150 mW for 10 minutes.

Non-treated biofilms were used as the control. Hundred microliters of bacterial biofilms were scraped and homogenized in 100 μl PBS. All homogenized samples were incubated with 1 μl 200-X ROS orange dye for 1 hour at 37 °C (Cellular ROS Assay kit (orange), ab186028). ROS was measured by flow cytometry (BD, Accuri C6). ROS levels were normalized with unstained biofilms and data were presented in percentage (%).

Confocal microscopy and SEM imaging

Biofilms were formed on 12 mm glass slides with the biofilm protocol mentioned above. For confocal microscopy, biofilms were fixed with 3.5% formaldehyde and mounted with DAPI (Mounting Medium with DAPI – Aqueous, Fluoroshield (ab104139)). Images were taken with a Leica DMI8 SP8 CS/DLS Microscope at 63× magnification. The excitation and emission wavelengths were 782 nm and 800 nm.

For SEM imaging, biofilms were fixed with 2.5% glutaraldehyde followed by gradual alcohol dehydration. Samples were covered with gold for 15 seconds after being exposed to vacuum. Images were taken using a Zeiss Evo LS15 Microscope at 2000 and 10 000× magnification.

Quantification of nanoparticle uptake

Internalization of nanoparticles was determined by a quantitative method based on the Fe content measured by ICP-MS. Planktonic cell cultures were treated with APTMS@SPIONs and ICG-APTMS@SPIONs with the abovementioned protocol. In order to remove free nanoparticles, bacterial suspensions were centrifuged and washed with 1× PBS. All liquid media were removed by gentle heating. Following the heating step, 1 ml of H_2SO_4 : HNO_3 (1 : 9) mixture was added to flasks and flasks were kept for 1 week for digestion.

Biofilms with APTMS@SPIONs and ICG-APTMS@SPIONs were prepared in sterile polystyrene 6-well plates and after overnight incubation, biofilms were washed with 1× PBS and then transferred to 10 ml flasks after scraping for 20 seconds. Once transferred to flasks, the protocol used for planktonic culture was adopted to prepare ICP samples. All samples were prepared as five replicates. Non-treated bacteria were included as the control group.

Statistical analysis

For statistical analysis, a one-way ANOVA test was used by Graphpad Prism Software (Graphpad Prism8). Free ICG and ICG-APTMS@SPIONs were compared with APTMS@SPIONs in terms of bacterial growth reduction and growth reduction was considered as statistically significant if $p < 0.05$.

Results

Synthesis and characterization of ICG-APTMS@SPIONs

APTMS@SPIONs and ICG-APTMS@SPIONs were prepared as described by Bilici *et al.*[41] APTMS@SPIONs were produced in a small hydrodynamic size and with strong positive surface charge (38 mV) (see Table 1). Electrostatic binding of ICG to APTMS@SPIONs was achieved with 14% EE and 1.4% LE. This reversed the surface charge (−44 mV) and increased the hydrodynamic size of nanoparticles to 35 nm, which is still considered as ultrasmall (Table 1). SPIONs lack strong specific absorbance in the NIR range, but ICG has two absorbance peaks at 710 nm and 780 nm, which are assigned to dimeric and monomeric ICG[46] (Fig. 2). ICG-APTMS@SPIONs exhibited two strong peaks at 810 nm and 710 nm, supporting ICG binding to SPIONs. About 30 nm redshift of the monomeric ICG peak may be due to the change in the chemical environment and to some degree of oligomer formation.[47]

Table 1 Properties of the nanoparticles

Sample name	Hydrodynamic size (nm)	ζ potential (mV)
APTMS@SPIONs	18	38
ICG-APTMS@SPIONs	35	−44

Antibacterial activity on planktonic cells

In the planktonic cells of all bacterial types treated with free ICG, APTMS@SPION, and ICG-APTMS@SPION, growth inhibition was not observed in the absence of laser irradiation (Fig. 3).

Colony counts of controls (without nanoparticle and laser) were found to be 1.19×10^{12} CFU ml^{-1} for *E. coli*, 9.67×10^{11} CFU ml^{-1} for *K. pneumoniae*, 1.67×10^{12} CFU ml^{-1} for *P. aeruginosa*, and 1.23×10^{10} CFU ml^{-1} for *S. epidermidis*. When combined with laser treatment, cationic APTMS@SPIONs caused complete inhibition of growth of *P. aeruginosa*, 7-log reduction in *E. coli* and no significant inhibition of *K. pneumoniae* and *S. epidermidis* planktonic cells. ICG alone or ICG-APTMS@SPIONs combined with laser treatment totally inhibited planktonic cells of all bacterial types. Killing activity of free ICG and ICG-APTMS@SPIONs under

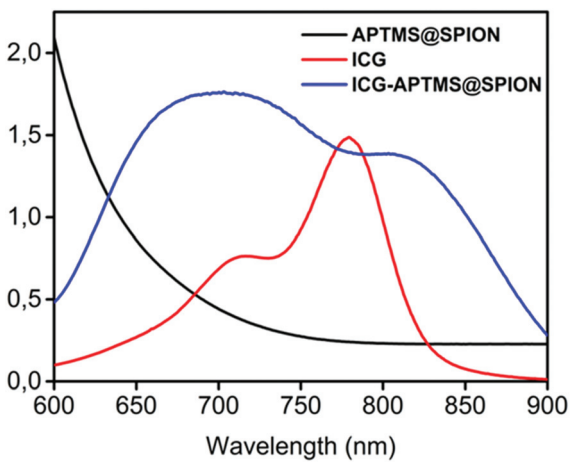

Fig. 2 UV-vis-absorption spectra of free ICG, APTMS@SPIONs and ICG-APTMS@SPIONs. ICG concentrations of ICG-APTMS@SPION and free ICG are identical (10 μg ICG per mL).

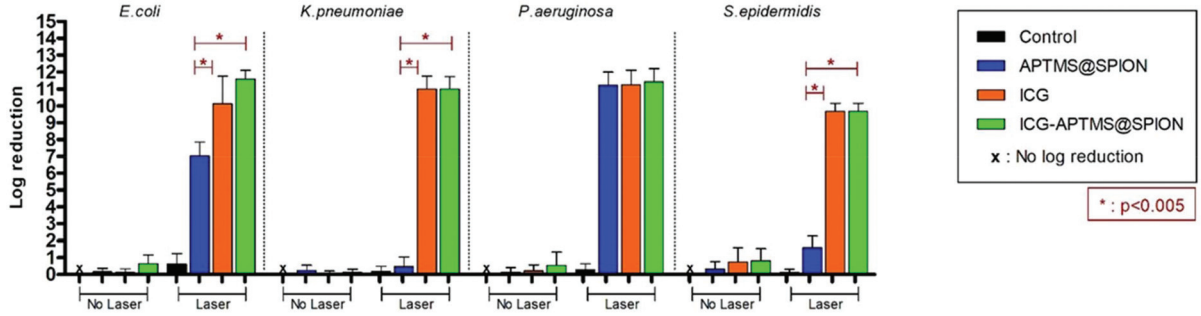

Fig. 3 Measured effect of APTMS@SPION (425 μg mL^{-1} Fe), ICG (25 μg ml^{-1}) and ICG-APTMS@SPION (25 μg ml^{-1} ICG or 425 μg mL^{-1} Fe) on the growth of planktonic cells with and without laser irradiation. Control: Planktonic cells were only treated with laser irradiation. All laser experiments were performed under 808 nm laser irradiation at 1150 mW for 10 min.

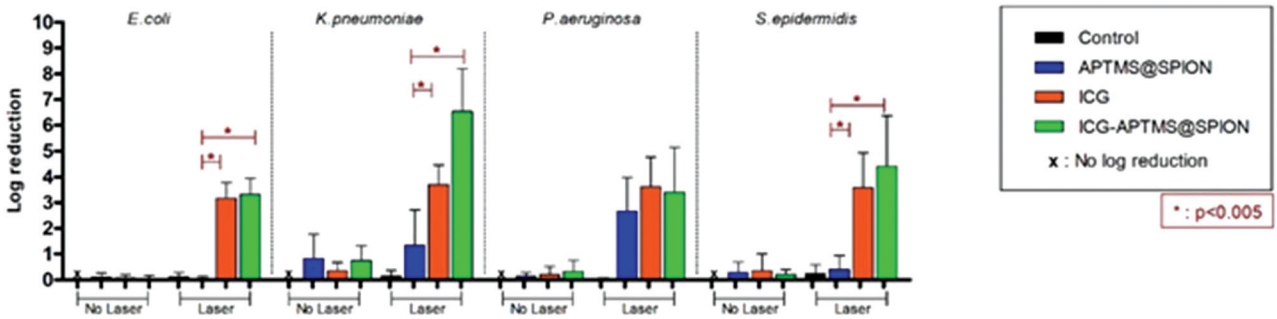

Fig. 4 Measured effect of APTMS@SPION (425 μg mL^{-1} Fe), ICG (25 μg ml^{-1}) and ICG-APTMS@SPION (25 μg ml^{-1} ICG or 425 μg mL^{-1} Fe) particles on growth of bacterial biofilms with and without laser irradiation. Control: Biofilms were only treated with laser irradiation. All laser experiments were performed under 808 nm laser irradiation at 1150 mW for 10 min.

laser treatment was significantly higher than that of APTMS@SPIONs ($p < 0.0001$) in all cases except *P. aeruginosa*.

Antibacterial activity on biofilms

Untreated biofilms (no laser, no photosensitizer) were used as controls. The mean growth of biofilm controls was 9.93×10^8 CFU ml^{-1}, 2.36×10^9 CFU ml^{-1}, 1.32×10^{10} CFU ml^{-1}, and 3.97×10^9 CFU ml^{-1} for *E. coli*, *K. pneumoniae*, *P. aeruginosa* and *S. epidermidis*, respectively. No significant inhibition was observed on biofilms treated with the APTMS@SPION, ICG and ICG-APTMS@SPIONs without laser treatment as in the case of planktonic cells (Fig. 4). APTMS@SPION/laser significantly reduced the *P. aeruginosa* biofilm (2.7-log reduction), but showed no significant inhibition on other bacterial biofilms. It was most influential on the *P. aeruginosa* biofilm in line with the results observed in the planktonic cells (Fig. 3). Free ICG/laser combination inhibited biofilms of *E. coli*, *K. pneumoniae*, *P. aeruginosa* and *S. epidermidis* with 3.2, 3.7, 3.6 and 3.6-log reductions, respectively. The ICG-APTMS@SPION/laser reduced biofilms in amounts comparable to ICG/laser again with 3.3, 3.4, 4.4-log reductions in *E. coli, P. aeruginosa and S. epidermidis*, respectively. Combination of dye and the nanoparticle in phototherapy was most effective on the *K. pneumoniae* biofilm with 6.5-log growth reduction. The reduction of the biofilm with ICG-APTMS@SPION/laser was always more effective than SPION@APTMS/laser, except in *P. aeruginosa*, wherein the difference in the growth inhibition of biofilms was not statistically significant between ICG (3.6-log), APTMS@SPIONs (2.7-log) andAPTMS@SPION/ICG (3.4-log).

Cellular uptake

The quantitative uptake of APTMS@SPIONs and ICG-APTMS@SPIONs by the biofilms and planktonic cells treated with these nanoparticles at 425 μg mL^{-1} [Fe] concentration for 24 h was determined with ICP-MS. Untreated cells were used as controls. Most planktonic cells internalize about 85% of the cationic APTMS@SPIONs and 98% of the anionic ICG-APTMS@SPIONs (Fig. 5a, b and d), except *P. aeruginosa* (Fig. 5c) where these values are about 70% and 80%, respectively. This may be due to the impermeable outer cell membrane of these bacteria, preventing penetration of nanoparticles more than others. Interestingly, these bacterial strains did not differentiate particles based on their surface charge in the case of planktonic cells. The largest difference between the APTMS@SPIONs and ICG-APTMS@SPIONs was *ca.* 10% in the case of *K. penumoniae* favoring the latter. ICG seems to enhance internalization of nanoparticles by both Gram-negative and Gram-positive bacteria.

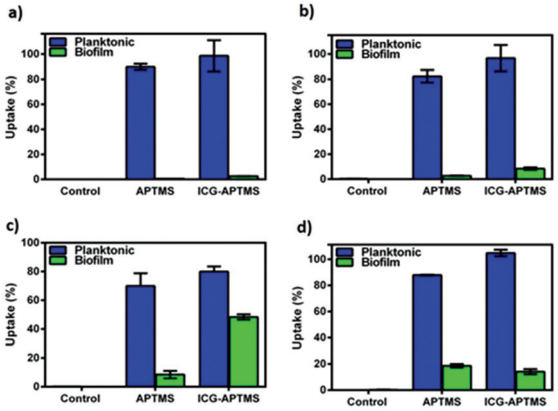

Fig. 5 Intracellular quantification of APTMS@SPIONs and ICG-APTMS@SPIONs in (a) *E. coli*, (b) *K. penumoniae*, (c) *P. aeruginosa* and (d) *S. epidermis*. Samples at 425 μg ml^{-1} Fe concentration were incubated with bacteria for 24 h. Intracellular Fe amounts were determined by ICP-MS.

Internalization of these NPs by biofilms was lower as expected (Fig. 5). Surprisingly, both NPs penetrate into biofilms of *P. aeruginosa* in the highest amount reaching 8 and 48% for APTMS@SPIONs and ICG-APTMS@SPIONs, respectively. This was followed by *S. epidermis* biofilms, which is the only Gram-positive strain, with about 18% internalization of both NPs. Penetration of nanoparticles to *K. penumoniae* and *E. coli* biofilms is relatively poor: below 10% and 5%, respectively.

Confocal microscopy images showed no attachment of ICG or ICG loaded NPs on *E. coli* but only few NP aggregates between the bacterial cells (Fig. 6a and b). On the other hand, few bacterial cells seem to be in interaction with the free ICG (Fig. 6c), but a significant enhancement in the interaction of ICG-APTMS@SPIONs with the *K. pneumoniae* biofilm was observed (Fig. 6d), which supports ICP-MS results. Actually, these microscopy images also demonstrate the ability of optical detection of the photosensitizer, which allows image-guided selection of the area for irradiation. In addition, free ICG or ICG-APTMS@SPION exposure without laser treatment did not cause any morphological changes in *E. coli* and *K. pneumoniae* biofilms which can be seen from the SEM images of the biofilms (Fig. S1†).

Temperature increase in the laser treated biofilms

A local temperature increase (ΔT) during laser irradiation of biofilms treated with APTMS@SPION, ICG and ICG-APTMS@SPIONs was recorded with a thermal camera as described above. Untreated cells were used as the control and the temperature differences of treated cells with respect to the control are displayed in Fig. 7.

APTMS@SPION/laser treatment caused the highest temperature increase by 20 °C in *S. epidermidis* which internalized more APTMS@SPIONs (*ca.* 18%) in comparison with others. The least uptake was detected in *E. coli* (*ca.* 0.4%) and the corresponding observed ΔT was 7.5 °C. *K. pneumoniae* picked

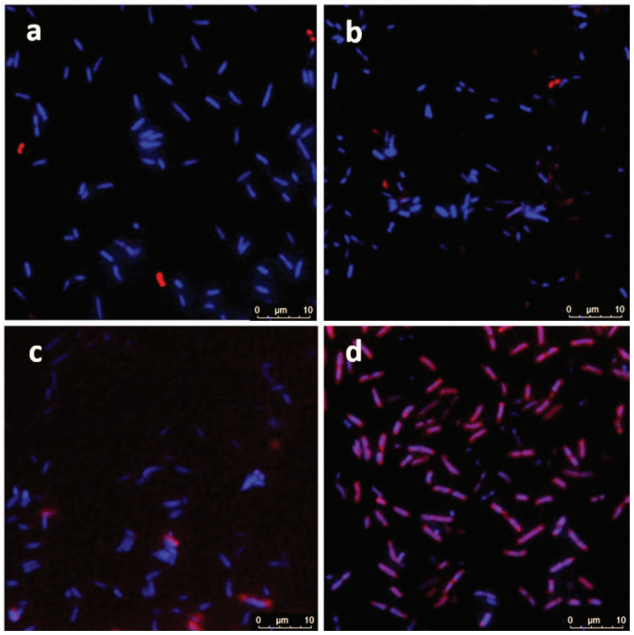

Fig. 6 Confocal microscopy images of bacterial biofilms: (a) *E. coli* biofilm with ICG, bacteria only (b) *E. coli* biofilm with ICG-APTMS@SPION bacteria only, (c) *K. pneumoniae* biofilm with ICG, nanoparticles slightly attached on bacterial cells and (d) *K. pneumoniae* biofilm with ICG-APTMS@SPION, nanoparticles attached on bacterial cells. Blue: Bacteria stained with DAPI: Red: Nanoparticles; 63× magnification.

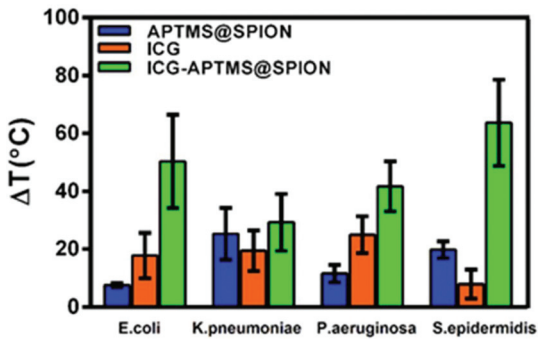

Fig. 7 Measured increase in the temperature (ΔT) of biofilms treated with an 808 nm laser (10 min, 1150 mW) with respect to the control (no treatment) as detected with a thermal camera. The data are expressed as the average of three experiments.

up 2.6% of the nanoparticles and experienced 25 °C temperature increase, while *P. aeruginosa* picked up 8.4% of the particles and experienced 12 °C temperature increase.

ICG/laser treatment caused higher temperature increases than APTMS@SPIONs (18–25 °C), except in *S. epidermidis* (8 °C). ICG-APTMS@SPION/laser showed significantly higher ΔT values than its components: *ca.* 50, 29, 42, 64 °C for *E. coli*, *K. pneumoniae*, *P. aeruginosa* and *S. epidermidis*, respectively. The highest uptake of ICG-APTMS@SPIONs was observed in *P. aeruginosa* (48%) but the highest temperate increase was

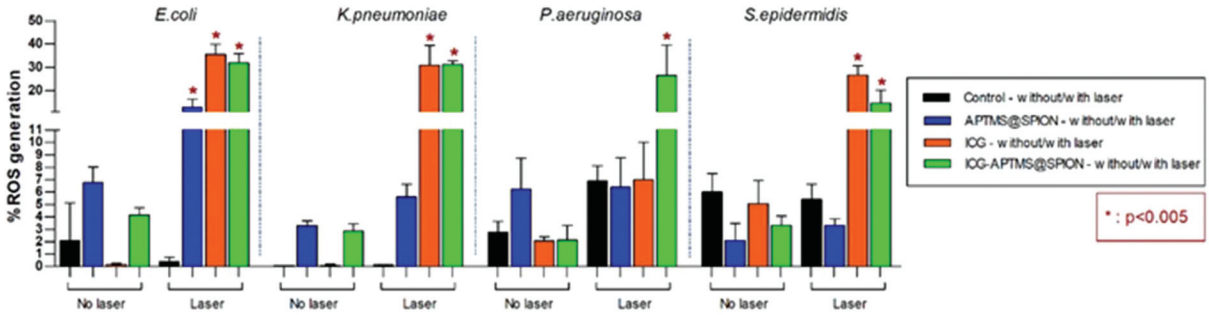

Fig. 8 Measured ROS levels of bacterial biofilms before and after 10 minutes of laser irradiation with 1150 mW.

observed in *S. epidermidis* which had about 14% nanoparticle uptake. This shows that different microbial strands respond to laser treatment differently.

ROS generation in biofilms upon laser irradiation

ROS levels for APTMS@SPION, ICG, and ICG-APTMS@SPION treated biofilms with/without laser irradiation are shown in Fig. 8. None of these photosensitizers causes significant ROS generation without laser irradiation. After laser treatment, when compared with control, all of the photosensitizers caused significantly higher ROS generation in *E. coli* biofilms with ROS levels around 12.8% with APTMS@SPIONs (p = 0.001), 35.6% with ICG (p < 0.0001), and 32.0% with ICG-APTMS@SPIONs (p < 0.0001). Indeed, APTMS@SPION/laser caused significant ROS generation only in *E. coli* biofilms. In *K. pneumoniae* biofilms, significant ROS generation was observed with ICG/laser (30.9%) and ICG@APTMS/laser (31.3%) (p < 0.0001), while in *P. aeruginosa* biofilms, only ICG-APTMS@SPION/laser caused a significantly increased (26.6%) ROS production (p < 0.0001). In *S. epidermidis* biofilms, ICG/laser caused 26.7% increase in ROS (p < 0.0001), while ICG-APTMS@SPION/laser caused 14.7% (p = 0.0072).

Discussions

Rapid increase of resistance to current antibiotics is a global threat and causes inefficient treatment especially for biofilm related infections.[1] As a result of limited therapy against resistant bacteria in biofilms, an urgent need for alternative options to antibiotics has risen. PDT and PTT were considered as a promising alternative and complementary therapy for some chemotherapy resistant cancers.[48,49] In recent years, adaptation of PDT and PTT for the treatment of multidrug resistant infections has shown quite successful results.[50–52]

In this study, we investigated the antimicrobial and antibiofilm effects of PDT/PTT combination using APTMS@SPION, ICG and ICG-APTMS@SPIONs and 10 min laser irradiation at 808 nm (output power of 1150 mW). We used three clinically important biofilm producing Gram negative bacteria (*K. pneumoniae*, *E. coli*, *P. aeruginosa*) and one Gram positive, strong biofilm producing bacteria, *S. epidermidis*, to assess the influence of surface charge on internalization of nanoparticles as well as the spectrum of PDT/PTT in different bacterial types.

We did not observe a significant antimicrobial effect in the planktonic cells of these bacteria types by any of these three photosensitizers in the absence of laser treatment. This indicates no dark toxicity related to these agents, but a significant phototoxic effect was detected after single, 10 minute irradiation of the treated cells at 808 nm. Overall, according to Fig. 3, after laser application: (1) *P. aeruginosa* and *E. coli* planktonic cells can be completely eliminated with any of these three agents, (2) APTMS@SPION/laser treatment showed a strong bactericidal effect but only on *P. aeruginosa* (with 11-log reduction of growth) and *E. coli* (7-log reduction), and (3) complete killing of *K. pneumoniae* and *S. epidermidis* planktonic cells was achieved with ICG and ICG-APTMS@SPION. This clearly shows that antimicrobial activity is not dependent on Gram-negative or Gram-positive cell wall nature of the bacteria when these photosensitizers are used. Cell internalization studies also indicate no strong dependence of this result on intracellular nanoparticle loading.

In a similar study, Topaloglu *et al.* reported a dose dependent bactericidal effect of ICG based PDT performed with an 809 nm laser on *P. aeruginosa* and *S. aureus* planktonic cells and achieved complete killing of *P. aeruginosa* with 125 μg mL^{-1} of ICG and 252 J cm^{-2} of light dose. In the case of *S. aureus*, 84 J cm^{-2} and 4 μg mL^{-1} ICG was sufficient for complete killing. Hence, they have suggested that the highly anionic cell-wall of Gram negative bacteria limited the interaction of anionic ICG with *P. aeruginosa.*[53] However, we have not seen a dramatic difference between the uptake of cationic APTMS@SPIONs or the anionic ICG loaded nanoparticles by Gram-negative or Gram-positive bacteria in this study, except in *S. epidermidis* (Gram-positive) which slightly favored anionic nanoparticles (Fig. 5). Omar *et al.* reported effective killing activity of ICG on planktonic cells of *P. aeruginosa*, *S. pyogenes* and *S. aureus* under 808 nm irradiation.[54] *S. pyogenes* and *S. aureus* treated with 25 μg ml^{-1} ICG and exposed to 411 J cm^{-2} (1.37 W cm^{-2}) of light intensity provided a 4.7-log and 5.5-log reduction in the viable cell count. However, 200 μg ml^{-1} ICG provided only a 2-log (99.1%) reduction in the viable cell count of *P. aeruginosa*. They have also reported no increase in the temperature of the bacterial suspensions, which is quite

usual for such laser doses, hence attributed the cell killing to PDT effect of ICG. Jijie *et al.* achieved complete killing of *E. coli* (6-log reduction) using 6 μM ICG loaded to Au nanoparticles and 3-log reduction with ICG free Au nanoparticles after 60 min pulsed laser irradiation at 810 nm with a laser intensity of 1 W cm^{-2} to eliminate PTT effect.[55] Phototoxicity of other dye-nanoparticle systems was also reported. For example, IR825 loaded pH sensitive zwitterionic fluorescent carbon dots (I-CD) provided 100% killing of planktonic *E. coli* and *S. aureus via* photothermal therapy at 10 mg mL^{-1} of I-CD after 5 min laser irradiation at 808 nm at pH 5.[56] In another example, photosensitization of tin-chlorin e6 conjugated gold nanoparticles under white light caused a hundred times more killing than free tin-chlorin on *S. aureus* after 10 min exposure.[57] Overall, the growth reduction obtained in our study is much higher compared to these reports despite low doses of the agents.

Here, we have achieved a complete killing of all planktonic cell types, both Gram-negative and Gram-positive, with only 25 μg mL^{-1} ICG or ICG loaded nanoparticles and irradiation at 808 nm (10 min) with 1150 mW (total energy of 690 J over 10 minutes) of laser power or 3 W cm^{-2} (total fluence of 1793 J cm^{-2} over 10 minutes) of irradiation fluence, which is strong enough to provide effective aPDT and aPTT. Also, we have achieved complete killing of *E. coli and P. aeruginosa* using APTMS@SPIONs (425 μg mL^{-1} Fe) under identical conditions. It is important to point out that in the absence of laser treatment, these agents did not cause any antimicrobial activity. Interestingly, Niemirowicz *et al.* reported 75%, 26% and 99% growth inhibition of *E. coli*, *P. aeruginosa*, *S. aureus* and *Candida albicans* when they treated the microorganisms with 2.5 mg mL^{-1} APTMS coated SPIONs for 24 h with no laser irradiation.[58] However, this is a quite high SPION dose compared to what was used here (425 μg mL^{-1}) and they have indeed used these nanoparticles to aggregate in the presence of such microorganisms to be separated from body fluids. There is no current study that combined APTMS@SPIONs and laser treatment; hence such significant killing activity of APTMS@SPIONs with NIR laser treatment on *P. aeruginosa* and *E. coli* is unique. Indeed, combination of these two findings may provide important guidelines and pave the way to diverse applications in the field of antimicrobial therapy.

Biofilms are much more difficult to treat due to limited penetration of therapeutic agents into the biofilm matrix. In this study, ICG and ICG-APTMS@SPION combination with laser treatment showed similar activity in all biofilms with 3.4–3.7-log reduction in colony counts, except in *S. epidermidis* and *K. pneumoniae*, where a 4.4 log reduction and a dramatic 6.5-log reduction were observed with the ICG-APTMS@SPION/laser. Similar to planktonic cells, APTMS@SPION/laser showed the highest antimicrobial activity in *P. aeruginosa* (2.7-log reduction), but no significant effect on other biofilms.

In order to elucidate the contribution of aPTT and aPDT, photogenerated ROS and local temperature increase were determined in irradiated biofilms which were treated with each photosensitizer. ROS generation of ICG and ICG-APTMS@SPIONs upon laser treatment was similar in all biofilms, except in *P. aeruginosa*, where free ICG did not increase the ROS level significantly. In this biofilm, a local temperature increase was 25 and 42 °C during ICG/laser and ICG-APTMS@SPION/laser treatment, respectively. ICG-SPION@APTMS/laser did not produce a significant amount of ROS in this biofilm, but resulted in a 12 °C temperature increase, which was enough for 2.7-log reduction in CFU. Therefore, these data suggest that *P. aeruginosa* is quite heat sensitive and the major bactericidal effect is due to aPTT in *P. aeruginosa*.

APTMS@SPION/laser produced a significant amount of ROS only in *E. coli*, which led to a 7.5 °C local temperature increase but did not cause any antimicrobial effect. Hence, this combination was ineffective for antimicrobial activity in *E. coli* biofilms. On the other hand, ICG/laser and ICG-APTMS@SPION/laser treatments produced similar ROS amounts in *E. coli* biofilms, leading to *ca.* 18 °C *versus* 50 °C temperature increase, respectively, and the resulting 3.2–3.3 log reduction in CFUs. These may suggest that *E. coli* is more sensitive to aPDT rather than aPTT and relatively high levels of ROS are needed for effective eradication of *E. coli* biofilms. However, since we observed a quite high reduction in biofilms for both cases, it is not possible to have a clear verdict on such differentiation between the killing mechanisms.

In *K. pneumoniae* biofilms, ΔT recorded for APTMS@SPION/laser was 25 °C with no accompanying ROS production, which resulted in no killing effect. ICG/laser and ICG-APTMS@SPION/laser treatments increased the temperature of the biofilms by 19 °C and 29 °C with comparable ROS amounts, but caused 3.7 and 6.5-log reductions, respectively. These suggest that only aPTT is not enough for successful eradication of this biofilm but ICG-APTMS@SPION/laser provides a dramatic bactericidal effect due to synergistic combination of aPTT/aPDT in *K. pneumoniae* biofilms. Compared to the *P. aeruginosa* biofilm, *K. pneumoniae* seems to be more heat resistant since no significant killing effect was observed by 25 °C temperature increase without ROS production in the latter, while only 12 °C increase provided 2.7-log reduction in the former. Probably, the thick polysaccharide capsule of this bacterium may cause some heat resistance. The increase of the local temperature may make the polysaccharide capsule more permeable and/or reduce the resistance of the bacteria to ROS, causing such an enhanced antimicrobial effect in combined aPTT/aPDT.

In *S. epidermidis* biofilms, strong antimicrobial activity was observed with ICG/laser and ICG-APTMS@SPION/laser, leading to 8 °C and 64 °C temperature increase and 35–25% ROS production, and causing 3.6- and 4.4-log reduction in CFUs, respectively. This indicates an enhanced bacteriocidal effect due to the combination of aPDT/aPTT. However, despite the 20 °C increase in temperature observed with APTMS@SPION/laser, neither a significant ROS generation nor

an accompanying antimicrobial activity was observed, suggesting that *S. epidermidis* is not very heat sensitive.

Conclusions

In this study, the bactericidal effect of PDT/PTT (808 nm, 1150 mW, 10 min) generated by excitation of free ICG, APTMS@SPION, and ICG-APTMS@SPIONs was investigated on both planktonic cells and biofilms of *P. aeruginosa*, *E. coli*, *K. pneumoniae* and *S. epidermidis.* We prepared small, stable and biocompatible cationic APTMS@SPIONs using a co-precipitation method and loaded ICG onto these cationic nanoparticles *via* electrostatic interactions to develop anionic ICG-APTMS@SPIONs. Preparation of these nanoparticles is quite simple and relatively inexpensive. None of these agents showed a bactericidal activity without laser irradiation at 25 μg mL^{-1} ICG dose, corresponding to a Fe concentration of 425 μg mL^{-1}. In the absence of these agents, laser irradiation did not cause an antimicrobial effect either. These prove that the laser treatment is safe and what we observe is aPDT/aPTT. A short-duration, single-wavelength laser treatment of the planktonic cells treated with ICG or ICG-APTMNS@SPION caused complete killing of the bacteria. But APTMS@SPION/laser showed a significant dependence on bacterial type and provided a strong killing activity only on *P. aeruginosa* and *E. coli.* This is the first report on such antibacterial phototoxicity of APTMS@SPION. This is quite valuable since these nanoparticles are usually well known in the literature as functional SPIONs. Cell internalization studies indicate no strong dependence of the results on intracellular nanoparticle loading or surface charge of the nanoparticles.

Combined aPDT/aPTT provided a more bactericidal effect in planktonic cells than biofilms, as expected. Overall, 3.3-log to 4.4-log reductions in CFUs were obtained after short-duration and single-wavelength laser treatment of ICG or ICG-APTMS@SPION treated biofilms. *S. epidermidis* biofilms appeared more vulnerable to aPDT requiring high ROS levels for effective eradication of biofilms. Here the synergistic effect of aPTT was not observed. *P. aeruginosa* biofilms were quite heat sensitive and were probably treated mostly with aPTT. In the case of *K. pneumoniae* biofilms, both aPTT and aPDT seem to be effective and the combination of both provided the complete eradication with 6.5-log reduction, which is the highest value among all, a quite high reduction ratio in the present literature as well.

Finally, we point out that aPDT/aPTT combination may be quite an effective alternative and local therapeutic method against resistant microbial infections even in the absence of an antibiotic agent. Besides, considering the current efforts in the development of new photosensitizer molecules and nanoparticles, we would like to point out that using existing well-known nanoparticles such as SPIONs and FDA approved ICG, which also enables image-guidance for the therapy, may shorten the path to clinical trials. Similar to "drug repurposing", there may be opportunities to re-purpose the dyes and nanoparticles that the community is familiar with.

Conflicts of interest

There are no conflicts of interest to declare.

Acknowledgements

This work was funded by TUBITAK (Project no. 118S547). The authors would like to thank Dr Barış Yağcı (KUYTAM, Koç University Surface Science and Technology Center), Dr Berna Morova (KUTTAM, Koç University Research Center for Translational Medicine) and Nesligül Yüksel Şentürk (KUTTAM, Koç University Research Center for Translational Medicine) for their help in various measurements and for recording microscope images.

References

1 A. Chatterjee, M. Modarai, N. R. Naylor, S. E. Boyd, R. Atun, J. Barlow, A. H. Holmes, A. Johnson and J. V. Robotham, *Lancet Infect. Dis.*, 2018, **18**, e368–e378.
2 N. Atac, O. Kurt-Azap, I. Dolapci, A. Yesilkaya, O. Ergonul, M. Gonen and F. Can, *Curr. Microbiol.*, 2018, **75**, 1661–1666.
3 B. Isler, Ş. Keske, M. Aksoy, Ö. K. Azap, M. Yilmaz, S. Ş. Yavuz, G. Aygün, E. Tigen, H. Akalın and A. Azap, *Clin. Microbiol. Infect.*, 2019, **25**, 651–653.
4 J. Y. Lee, I. R. Monk, A. G. da Silva, T. Seemann, K. Y. Chua, A. Kearns, R. Hill, N. Woodford, M. D. Bartels and B. Strommenger, *Nat. Microbiol.*, 2018, **3**, 1175–1185.
5 V. R. Buford, V. Kumar and B. R. Kennedy, *Am. J. Infect. Control*, 2016, **44**, 381–386.
6 H. C. Flemming and J. Wingender, *Nat. Rev. Microbiol.*, 2010, **8**(9), 623–633.
7 J. Iredell, J. Brown and K. Tagg, *Br. Med. J.*, 2016, **352**, h6420.
8 P. Agostinis, K. Berg, K. A. Cengel, T. H. Foster, A. W. Girotti, S. O. Gollnick, S. M. Hahn, M. R. Hamblin, A. Juzeniene and D. Kessel, *CA-Cancer J. Clin.*, 2011, **61**, 250–281.
9 D. E. Dolmans, D. Fukumura and R. K. Jain, *Nat. Rev. Cancer*, 2003, **3**, 380–387.
10 D. Jaque, L. M. Maestro, B. Del Rosal, P. Haro-Gonzalez, A. Benayas, J. Plaza, E. M. Rodriguez and J. G. Sole, *Nanoscale*, 2014, **6**, 9494–9530.
11 A. C. Tedesco, F. L. Primo and P. d. C. C. de Jesus, in *Multifunctional Systems for Combined Delivery, Biosensing and Diagnostics*, Elsevier, 2017, pp. 9–29.
12 M. R. Hamblin, *Curr. Opin. Microbiol.*, 2016, **33**, 67–73.
13 V. Pérez-Laguna, L. Pérez-Artiaga, V. Lampaya-Pérez, I. García-Luque, S. Ballesta, S. Nonell, M. P. Paz-Cristobal, Y. Gilaberte and A. Rezusta, *Front. Microbiol.*, 2017, **8**, 1002.

14 W. C. De Melo, P. Avci, M. N. De Oliveira, A. Gupta, D. Vecchio, M. Sadasivam, R. Chandran, Y.-Y. Huang, R. Yin and L. R. Perussi, *Expert Rev. Anti-Infect. Ther.*, 2013, **11**, 669–693.
15 X. Hu, Y.-Y. Huang, Y. Wang, X. Wang and M. R. Hamblin, *Front. Microbiol.*, 2018, **9**, 1299.
16 W. Li, X. Geng, D. Liu and Z. Li, *Int. J. Nanomed.*, 2019, **14**, 8047.
17 J. C. Castillo-Martínez, G. A. Martínez-Castañón, F. Martínez-Gutierrez, N. V. Zavala-Alonso, N. Patiño-Marín, N. Niño-Martinez, V. Zaragoza-Magaña and C. Cabral-Romero, *J. Nanomater.*, 2015, **2015**, 783671.
18 J.-W. Xu, K. Yao and Z.-K. Xu, *Nanoscale*, 2019, **11**, 8680–8691.
19 A. G. Al-Bakri and N. N. Mahmoud, *Molecules*, 2019, **24**, 2661.
20 T. Ibelli, S. Templeton and N. Levi-Polyachenko, *Int. J. Hyperthermia*, 2018, **34**, 144–156.
21 B. Chen, Y. Sun, J. Zhang, R. Chen, X. Zhong, X. Wu, L. Zheng and J. Zhao, *Front. Microbiol.*, 2019, **10**, 1228.
22 J. Malicka, I. Gryczynski, C. D. Geddes and J. R. Lakowicz, *J. Biomed. Opt.*, 2003, **8**, 472.
23 J.-M. I. Maarek, D. P. Holschneider and J. Harimoto, *J. Photochem. Photobiol., B*, 2001, **65**, 157–164.
24 Z. Li, S. Yao and J. Xu, *Sci. Rep.*, 2019, **9**, 1–8.
25 F. An, Z. Yang, M. Zheng, T. Mei, G. Deng, P. Guo, Y. Li and R. Sheng, *J. Nanobiotechnol.*, 2020, **18**, 1–11.
26 D. Wu, Z. Zhao, N. Wang, X. Zhang, H. Yan, X. Chen, Y. Fan, W. Liu and X. Liu, *Biomater. Sci.*, 2020, **8**, 3443–3453.
27 N. Lee and T. Hyeon, *Chem. Soc. Rev.*, 2012, **41**, 2575–2589.
28 A.-K. Kirchherr, A. Briel and K. Mäder, *Mol. Pharm.*, 2009, **6**, 480–491.
29 V. Saxena, M. Sadoqi and J. Shao, *J. Pharm. Sci.*, 2003, **92**, 2090–2097.
30 V. Saxena, M. Sadoqi and J. Shao, *J. Photochem. Photobiol., B*, 2004, **74**, 29–38.
31 W. Li, H. Zhang, X. Guo, Z. Wang, F. Kong, L. Luo, Q. Li, C. Zhu, J. Yang and Y. Lou, *ACS Appl. Mater. Interfaces*, 2017, **9**, 3354–3367.
32 P. Xue, R. Yang, L. Sun, Q. Li, L. Zhang, Z. Xu and Y. Kang, *Nano-Micro Lett.*, 2018, **10**, 74.
33 M. Yin, Z. Li, E. Ju, Z. Wang, K. Dong, J. Ren and X. Qu, *Chem. Commun.*, 2014, **50**, 10488–10490.
34 E. Zhang and C. Zou, *Acta Biomater.*, 2009, **5**, 1732–1741.
35 M. Li, L. Li, K. Su, X. Liu, T. Zhang, Y. Liang, D. Jing, X. Yang, D. Zheng and Z. Cui, *Adv. Sci.*, 2019, **6**, 1900599.
36 K. Jibin, J. Prasad, G. Saranya, S. J. Shenoy, K. K. Maiti and R. S. Jayasree, *Biomater. Sci.*, 2020, **8**, 3381–3391.
37 J. Zhang, S. Rana, R. Srivastava and R. Misra, *Acta Biomater.*, 2008, **4**, 40–48.
38 C. Sun, J. S. Lee and M. Zhang, *Adv. Drug Delivery Rev.*, 2008, **60**, 1252–1265.
39 Z. Zhou, Y. Sun, J. Shen, J. Wei, C. Yu, B. Kong, W. Liu, H. Yang, S. Yang and W. Wang, *Biomaterials*, 2014, **35**, 7470–7478.
40 M. Chu, Y. Shao, J. Peng, X. Dai, H. Li, Q. Wu and D. Shi, *Biomaterials*, 2013, **34**, 4078–4088.
41 K. Bilici, A. Muti, A. Sennaroğlu and H. Y. Acar, *J. Photochem. Photobiol., B*, 2019, **201**, 111648.
42 K. Niemirowicz, U. Surel, A. Z. Wilczewska, J. Mystkowska, E. Piktel, X. Gu, Z. Namiot, A. Kułakowska, P. B. Savage and R. Bucki, *J. Nanobiotechnol.*, 2015, **13**, 32.
43 L. M. Armijo, S. J. Wawrzyniec, M. Kopciuch, Y. I. Brandt, A. C. Rivera, N. J. Withers, N. C. Cook, D. L. Huber, T. C. Monson and H. D. Smyth, *J. Nanobiotechnol.*, 2020, **18**, 1–27.
44 M. Arakha, S. Pal, D. Samantarrai, T. K. Panigrahi, B. C. Mallick, K. Pramanik, B. Mallick and S. Jha, *Sci. Rep.*, 2015, **5**, 14813.
45 J. Merritt, D. Kadouri and G. O'Toole, *Growing and Analyzing Static Biofilms*, *John Wiley & Sons*, 2005.
46 R. Liu, J. Tang, Y. Xu, Y. Zhou and Z. Dai, *Nanotheranostics*, 2017, **1**, 430.
47 X. Tan, J. Wang, X. Pang, L. Liu, Q. Sun, Q. You, F. Tan and N. Li, *ACS Appl. Mater. Interfaces*, 2016, **8**, 34991–35003.
48 B. Liu, C. Li, G. Chen, B. Liu, X. Deng, Y. Wei, J. Xia, B. Xing, P. a. Ma and J. Lin, *Adv. Sci.*, 2017, **4**, 1600540.
49 W.-H. Jian, T.-W. Yu, C.-J. Chen, W.-C. Huang, H.-C. Chiu and W.-H. Chiang, *Langmuir*, 2015, **31**, 6202–6210.
50 M. Valenzuela-Valderrama, I. A. González and C. E. Palavecino, *Photodiagn. Photodyn. Ther.*, 2019, **28**, 256–264.
51 C. Beltes, H. Sakkas, N. Economides and C. Papadopoulou, *Photodiagn. Photodyn. Ther.*, 2017, **17**, 5–8.
52 G. Qing, X. Zhao, N. Gong, J. Chen, X. Li, Y. Gan, Y. Wang, Z. Zhang, Y. Zhang and W. Guo, *Nat. Commun.*, 2019, **10**, 1–12.
53 N. Topaloglu, M. Gulsoy and S. Yuksel, *Photomed. Laser Surg.*, 2013, **31**, 155–162.
54 G. S. Omar, M. Wilson and S. P. Nair, *BMC Microbiol.*, 2008, **8**, 111.
55 R. Jijie, T. Dumych, L. Chengnan, J. Bouckaert, K. Turcheniuk, C.-H. Hage, L. Heliot, B. Cudennec, N. Dumitrascu and R. Boukherroub, *J. Mater. Chem. B*, 2016, **4**, 2598–2605.
56 E. B. Kang, P. T. M. Phuong, G. Lee, S. Lee, I. In and S. Y. Park, *Macromol. Res.*, 2019, **27**, 720–728.
57 J. Gil-Tomás, L. Dekker, N. Narband, I. P. Parkin, S. P. Nair, C. Street and M. Wilson, *J. Mater. Chem.*, 2011, **21**, 4189–4196.
58 K. Niemirowicz, I. Swiecicka, A. Z. Wilczewska, K. H. Markiewicz, U. Surel, A. Kułakowska, Z. Namiot, B. Szynaka, R. Bucki and H. Car, *Colloids Surf., B*, 2015, **131**, 29–38.